ELSEVIER

Journal of Power Sources 108 (2002) 97–105

JOURNAL OF POWER SOURCES

www.elsevier.com/locate/jpowsour

Microstructure and cycling behavior of $LiAl_{0.1}Mn_{1.9}O_4$ cathode for lithium secondary batteries at 3 V

S.G. Youn[a], I.H. Lee[a], C.S. Yoon[a,*], C.K. Kim[a], Yang-Kook Sun[b], Yun-Sung Lee[c], Masaki Yoshio[c]

[a]*Department of Materials Science and Engineering, Hanyang University, Seoul 133-791, South Korea*
[b]*Department of Industrial Chemistry, Hanyang University, Seoul 133-791, South Korea*
[c]*Department of Applied Chemistry, Saga University, 1 Honjo, Saga 840-8502, Japan*

Received 2 August 2001; accepted 15 December 2001

Abstract

$LiAl_{0.1}Mn_{1.9}O_4$ is synthesized using three different Mn-precursors through solid-state sintering. Although the powder structures of $LiAl_{0.1}Mn_{1.9}O_4$ appear to be identical when examined by powder X-ray diffraction (XRD) analysis, the reversible capacity ranges from 50 to 120 mAh g^{-1}, depending on the Mn-precursor, when cycled from 2.2 to 3.6 V. Transmission electron microscopy (TEM) structural analysis shows that there are subtle differences among the microstructures of the as-prepared powders. Although all three powders exhibit capacity fade, typical of the spinel material at 3 V, it is found that the particle size and morphology, as well as the structural difference, play an important role in improving or further degrading the cycling behavior of the spinel material.

Keywords: Lithium secondary batteries; Electrochemical cycling; Cathode material; Spinel

1. Introduction

$LiMn_2O_4$ with a normal spinel structure ($Fd\bar{3}m$) has recently received much attention as the cathode material for lithium rechargeable batteries because of the low cost and the non-toxicity of the manganese [1–3]. Unfortunately, it has not proved successful to substitute $LiCoO_2$ with spinel $LiMn_2O_4$ due to the gradual degradation of its capacity on cycling. It has been suggested that this capacity fading is due to spinel dissolution [4], the Jahn–Teller effect [2], and/or lattice instability [5].

Generally, the discharge curve of the $Lil Li_xMn_2O_4$ cell exhibits two voltage plateaux. For $0 \leq x \leq 1$, the cell discharges at 4 V versus Li/Li^+, whereas for $1 \leq x \leq 2$, the cells discharge at 3 V versus Li/Li^+ [6,7]. In the 3 V range, a large capacity fading with cycling is encountered as the Jahn–Teller distortion caused by Mn^{3+} ions induces a crystal symmetry change from cubic to tetragonal during the lithium insertion. The transformation leads to a volume change that is sufficiently large to destroy the structural integrity of the material. In order to improve the cycling performance of the spinel electrode, several researchers have attempted to substitute a small fraction of the manganese ions with other metal cations. Recently, cobalt and chromium doped $LiMn_2O_4$ spinels synthesized by a solid-state reaction have been reported [8,9] to show substantial improvement in cycle-life without dramatically sacrificing initial capacity. The improvement has been attributed to the partial substitution of the manganese ion in the 16d octahedral site, which enhances the overall structural stability of the material. Zhang et al. [10] have reported that chromium dopant also enhances the mass transfer of Li^+ in the active material.

The lithium intercalation properties of $LiAl_xMn_{2-x}O_4$ have been reported by Le Cras et al. [11]. Since aluminum is light in weight, abundant and relatively inexpensive, Al-substituted manganese spinel is expected to be a cathode material with higher specific energy, lower cost, and less toxicity. Park et al. [12] reported that a Al-doped spinel electrode ($Li_{1.02}Al_{0.25}Mn_{1.75}O_4$) exhibited no capacity loss after 30 cycles in both the 3 and 4 V regions during cycling. In addition, Song et al. [13] reported that cathodes based on substituting a part of Mn with Al and Cr give a good cycle-life in spite of some decrease in initial capacity, and the chemical diffusion coefficient of lithium ions in the cathode is increased by the doping.

In this study, we have substituted a part of the manganese with aluminum to examine the effects of particle morphology and microstructural differences on the cycling behavior of $LiAl_{0.1}Mn_{1.9}O_4$ in the 3 V range. Powders with different

* Corresponding author. Tel.: +82-2-2290-0409; fax: +82-2-2290-1838.
E-mail address: csyoon@hanyang.ac.kr (C.S. Yoon).

0378-7753/02/$ – see front matter
PII: S0378-7753(01)01080-1

morphology and microstructure are synthesized using three different Mn-precursors.

2. Experimental procedure

$LiAl_{0.1}Mn_{1.9}O_4$ was synthesized through solid-state sintering using reagent grade, LiOH, $Al(NO_3)_3$ (Katayama Chemical, Japan) and three different Mn-precursors: Mn_3O_4 (Brownox®-X, Tosoh, Japan), Mn_3O_4 (Juho, Japan), and γ-MnOOH (Tosoh, Japan). A stoichiometric amount of each material is mixed and pre-calcined at 470 and 530 °C for 5 h in oxygen and further calcined at 800 °C for 24 h in air. The chemical composition of the resulting powder was analyzed with an inductively coupled plasma (ICP) spectrometer by dissolving the powder dilute nitric acid.

Electrochemical cycling was performed using a CR2032 coin-type cell. The cathode consisted of 20 mg of accurately weighed active material and 13 mg of conductive binder. The material was pressed on a 25 mm^2 stainless-steel mesh, which was used as a current-collector, under a pressure of 300 kg cm^{-2} and dried at 200 °C for 5 h. The test cell was constructed using the cathode and a lithium metal anode (Cyprus Foote Mineral Co.) which were separated by a porous polypropylene film (Celgard 3401). The electrolyte was a mixture of 1 M $LiPF_6$–ethylene carbonate (EC)/dimethyl carbonate (DMC) (1:2 by volume). The charge-discharge current density was maintained at 0.4 mA cm^{-2} with cut-off voltages of 2.2–3.6 V.

To investigate the structural changes of the cathode material after the cycling, the test cell was left in a dry room for 2 days to reach equilibrium after the fully discharged state, and washed with DMC solution to remove the remaining $LiPF_6$ salt.

The powder X-ray diffraction (XRD) (Rigaku, Japan) using Cu Kα radiation and a transmission electron microscope (TEM), (JEM2010, JOEL, Japan) equipped with an energy-dispersive X-ray spectrometer (EDS) were employed to characterize the microstructure of the powder before and after the electrochemical cycling.

3. Results and discussion

The XRD patterns of the synthesized powders using different precursors before electrochemical cycling are presented in Fig. 1. As can be seen from the XRD patterns and Rietveld refining [14], the powders have nearly perfect

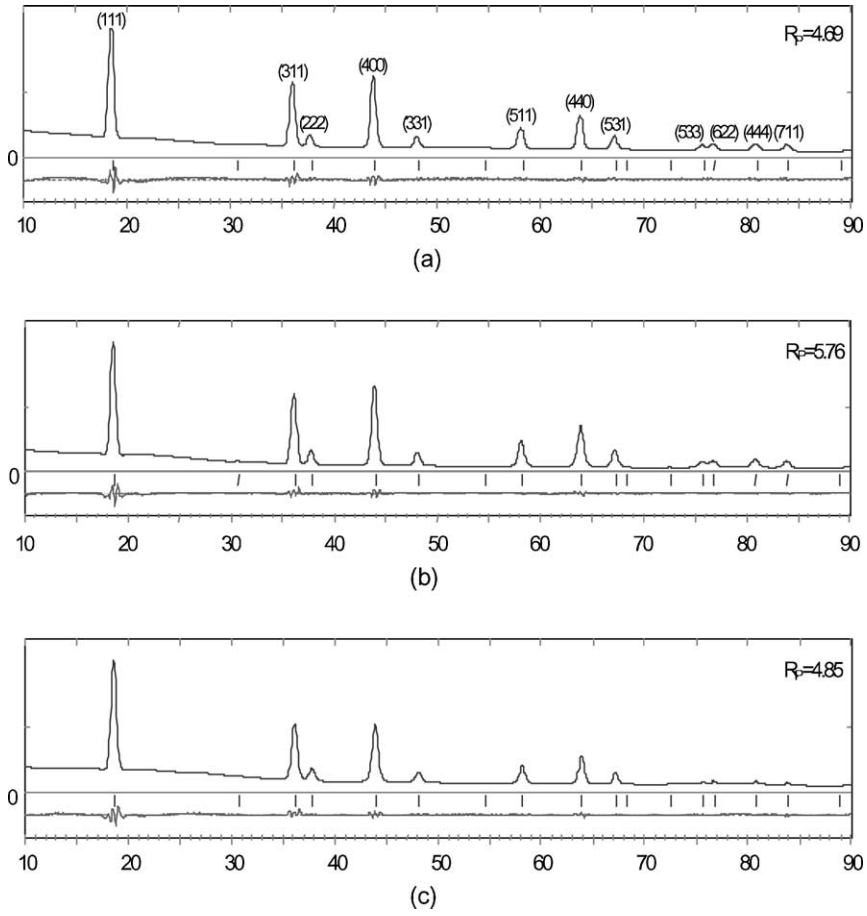

Fig. 1. XRD patterns with Rietveld refinement of $LiAl_{0.1}Mn_{1.9}O_4$ powder before electrochemical cycling: (a) t-$LiAl_{0.1}Mn_{1.9}O_4$; (b) j-$LiAl_{0.1}Mn_{1.9}O_4$; (c) γ-$LiAl_{0.1}Mn_{1.9}O_4$.

spinel structures. Although the powders are produced by means of identical process and appear to have a similar structure, the morphology of the powders is strikingly different, as can be seen in the SEM images of the three spinel powders in Fig. 2. The $LiAl_{0.1}Mn_{1.9}O_4$ powder based on Tosoh Mn_3O_4 (herein referred to as t-$LiAl_{0.1}Mn_{1.9}O_4$) has much smaller particle size (in sub-micron range) compared with $LiAl_{0.1}Mn_{1.9}O_4$ powder produced from Juho Mn_3O_4 (herein referred to as j-$LiAl_{0.1}Mn_{1.9}O_4$), whose particle size is estimated to be ∼1 μm. Particles of the $LiAl_{0.1}Mn_{1.9}O_4$ with γ-MnOOH precursor (herein referred to as γ-$LiAl_{0.1}Mn_{1.9}O_4$) have an elongated, acicular shape, unlike the other two powders. The different powder structures stem from the morphology of the Mn-precursor as Tosoh Mn_3O_4 has much finer particle size (∼0.1 μm), whereas Juho Mn_3O_4 has a particle size of ∼1 μm prior to the spinel powder synthesis. γ-$LiAl_{0.1}Mn_{1.9}O_4$ also appears to have retained its initial particle shape.

A bright field TEM image of the t-$LiAl_{0.1}Mn_{1.9}O_4$ powder prior to the electrochemical cycling is presented in Fig. 3. It

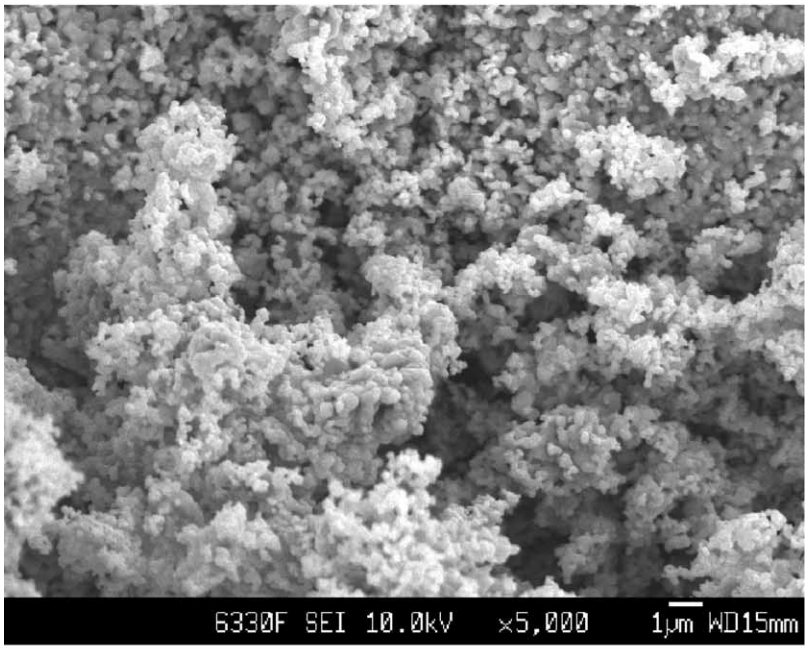

(a)

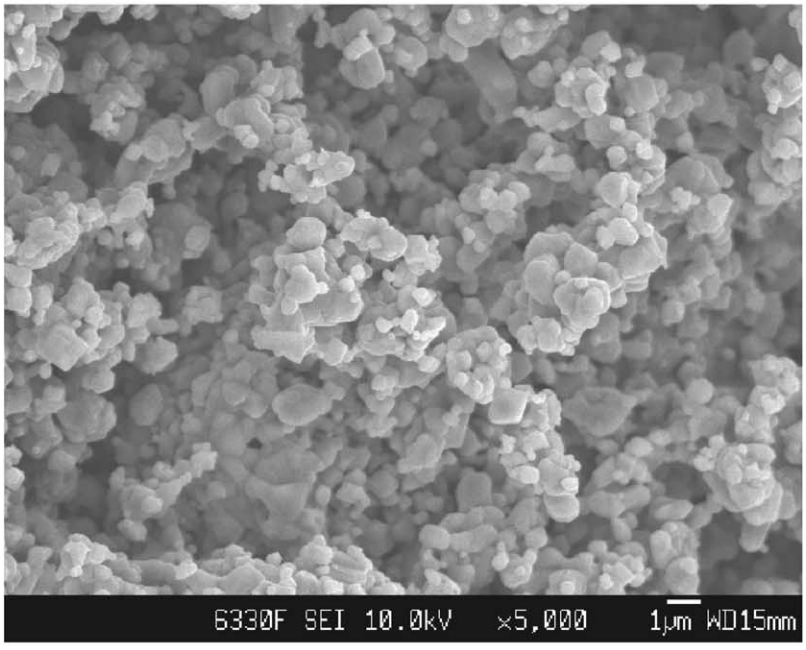

(b)

Fig. 2. SEM images of $LiAl_{0.1}Mn_{1.9}O_4$ powder before electrochemical cycling: (a) t-$LiAl_{0.1}Mn_{1.9}O_4$; (b) j-$LiAl_{0.1}Mn_{1.9}O_4$; (c) γ-$LiAl_{0.1}Mn_{1.9}O_4$.

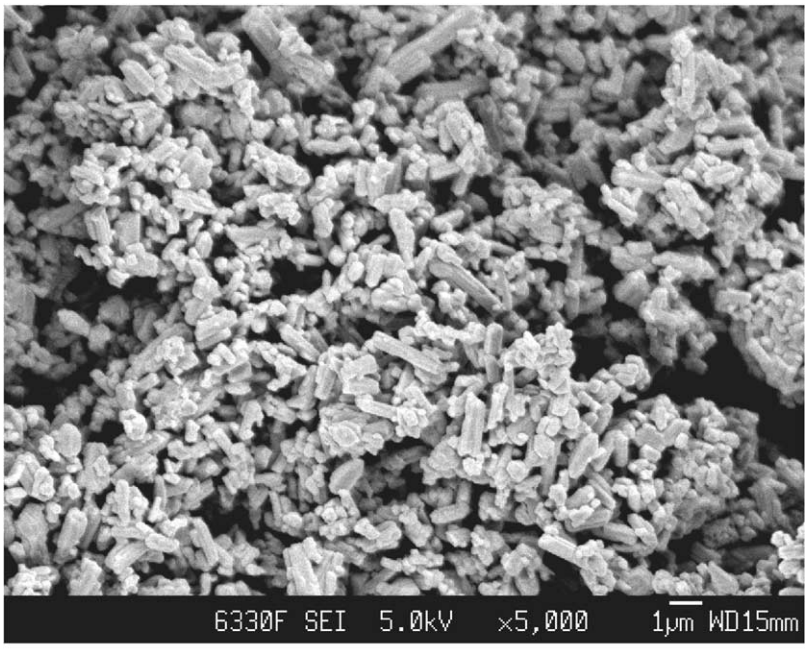

(c)

Fig. 2. (*Continued*).

is seen that t-$LiAl_{0.1}Mn_{1.9}O_4$ consists of 200 nm sized, equiaxed, spinel crystals. The electron diffraction pattern of a single particle in the [1 1 1] zone is shown in Fig. 3b. It shows good crystallinity of synthesized material. Compared with t-$LiAl_{0.1}Mn_{1.9}O_4$, j-$LiAl_{0.1}Mn_{1.9}O_4$ has a much larger particle size, as shown in Fig. 4a, which agrees with SEM data. The electron diffraction pattern of a single particle in the [1 1 0] zone is shown if Fig. 4b.

Although XRD results indicate that γ-$LiAl_{0.1}Mn_{1.9}O_4$ is made up of pure spinel crystals, TEM analysis shows that the powder is composed of multiple phases with different shapes. Some of the elongated particles are tetragonal (or monoclinic) crystals intermixed with equiaxed spinel crystal, as shown in Fig. 5. Close examination of the SEM image in Fig. 2c also confirms the existence of two types of particle shapes. The indexed electron diffraction patterns of each phase are given in Fig. 5b–d. Analysis of the electron diffraction indicate that the structure of the tetragonal elongated particles for γ-$LiAl_{0.1}Mn_{1.9}O_4$ have $c/a = 1.7$ and a [0 0 1] (along the long-axis) preferred growth orientation. The elongated particle is also found to be a monoclinic phase, as shown in Fig. 5d, and the phase has lattice parameters of $a = 5.4$ Å and $c = 5.4$ Å with $\beta = 116^\circ$. It is surprising that a tetragonal or monoclinic phase is formed during the synthesis process. It is known, however, that a lower symmetry structure of lithium manganese oxide can be prepared by reacting γ-MnOOH with LiOH in a reducing atmosphere [15]. It is also possible that during the calcination process, a local defiency of oxygen has generated Mn^{3+} (Jahn–Teller) ions which result in tetragonal transformation of the spine phase [16]. It is not clear why XRD data did not show the tetragonal (or monoclinic phase) phase, but it is possible that the strong texture and improper sample preparation could have erased some of the strong tetragonal peaks.

A comparison of the voltage curves for t-$LiAl_{0.1}Mn_{1.9}O_4$, j-$LiAl_{0.1}Mn_{1.9}O_4$ and γ-$LiAl_{0.1}Mn_{1.9}O_4$ during 50 discharge–charge cycles is given in Fig. 6. t-$LiAl_{0.1}Mn_{1.9}O_4$ exhibits a large initial reversible capacity of 125 mAh g^{-1} which rapidly drops to 40 mAh g^{-1} at the end of 50 electrochemical cycles. Meanwhile, the j-$LiAl_{0.1}Mn_{1.9}O_4$ powder has a slightly lower initial capacity of 110 mAh g^{-1} which gradually decreases to give a reversible capacity fade of ∼10 mAh g^{-1} after 50 cycles. The γ-$LiAl_{0.1}Mn_{1.9}O_4$ had the largest initial reversible capacity of 130 mAh g^{-1}, but the capacity slowly decreases to 100 mAh g^{-1} after 50 cycles. Although j-$LiAl_{0.1}Mn_{1.9}O_4$ electrode has the lowest initial capacity, the powder exhibits the best capacity retention during cycling. Depending on the source of the Mn-precursor, very different cycling behavior is observed. Also noted in the voltage curves for all three powders is the flat voltage level during cycling. This suggests the existence of two phases which arise from the Jahn–Teller distortion [17].

XRD is used to analyze the powder structure after cycling and the resulting data indicated the formation of secondary phases. It was rather inconclusive, however, regarding the structure of the secondary phases. In fact, the tetragonal and monoclinic phases are nearly indistinguishable with XRD [18]. Hence, the particle structures were studied using TEM after the electrochemical cycling, and the identified structure of the individual particles is listed in Table 1. After 50 electrochemical cycles, the powders contain the tetragonal phase or the monoclinic phase formed through Jahn–Teller distortion at 3 V [19]. The phase transformation and the

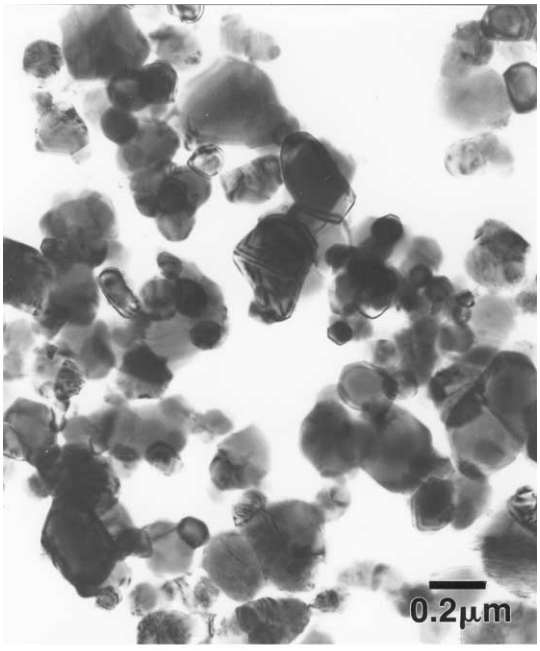

Fig. 3. (a) TEM bright field image of t-$LiAl_{0.1}Mn_{1.9}O_4$ powder before cycling; (b) electron diffraction pattern of a t-$LiAl_{0.1}Mn_{1.9}O_4$ single spinel particle before cycling in [1 1 1] zone.

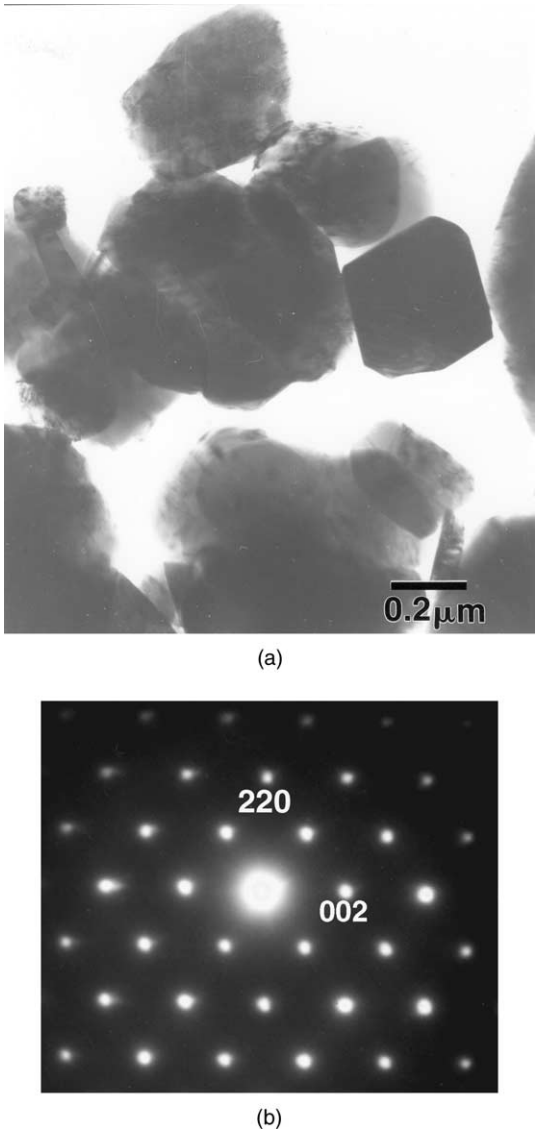

Fig. 4. (a) TEM bright field image of j-$LiAl_{0.1}Mn_{1.9}O_4$ powder before cycling; (b) electron diffraction pattern of j-$LiAl_{0.1}Mn_{1.9}O_4$ spinel particle before cycling in [1 1 0] zone.

accompanying capacity fade are consistent with the previously reported results for a $LiAl_{0.24}Mn_{1.76}O_4$ cathode [20].

Typical electron diffraction patterns found after cycling t-$LiAl_{0.1}Mn_{1.9}O_4$ are given in Fig. 7a–c. The diffraction patterns do not indicate any significant distortion of the lattice (no satellite or split peaks) when compared with the initial diffraction patterns. t-$LiAl_{0.1}Mn_{1.9}O_4$ powder exhibits, however, much higher capacity loss when cycled between 2.4 and 3.5 V compared with j-$LiAl_{0.1}Mn_{1.9}O_4$ and γ-$LiAl_{0.24}Mn_{1.76}O_4$. The rapid loss of capacity can be attributed to the comparatively small particle size of the t-$LiAl_{0.1}Mn_{1.9}O_4$ powder which led to enhanced acid attack from the electrolyte and the following surface reaction [21]:

$$2Mn^{3+}(\text{solid}) \rightarrow Mn^{4+}(\text{solid}) + Mn^{2+}(\text{solution}) \quad (1)$$

such reaction and acid attack will dissolve the spinel electrode and cause the capacity to fade. In addition, the ratio of the spinel/tetragonal phases is lowest compared with the other two powders. Although the ratio may not be statistically significant due to the small sampling size, it can be

Table 1
Structure of individual particles studied by means of TEM

	t-$LiAl_{0.1}Mn_{1.9}O_4$	j-$LiAl_{0.1}Mn_{1.9}O_4$	γ-$LiAl_{0.1}Mn_{1.9}O_4$
Total number of particles	10	11	12
Cubic spinel	4	8	8
Tetragonal	4	–	4
Monoclinic	2	3	–

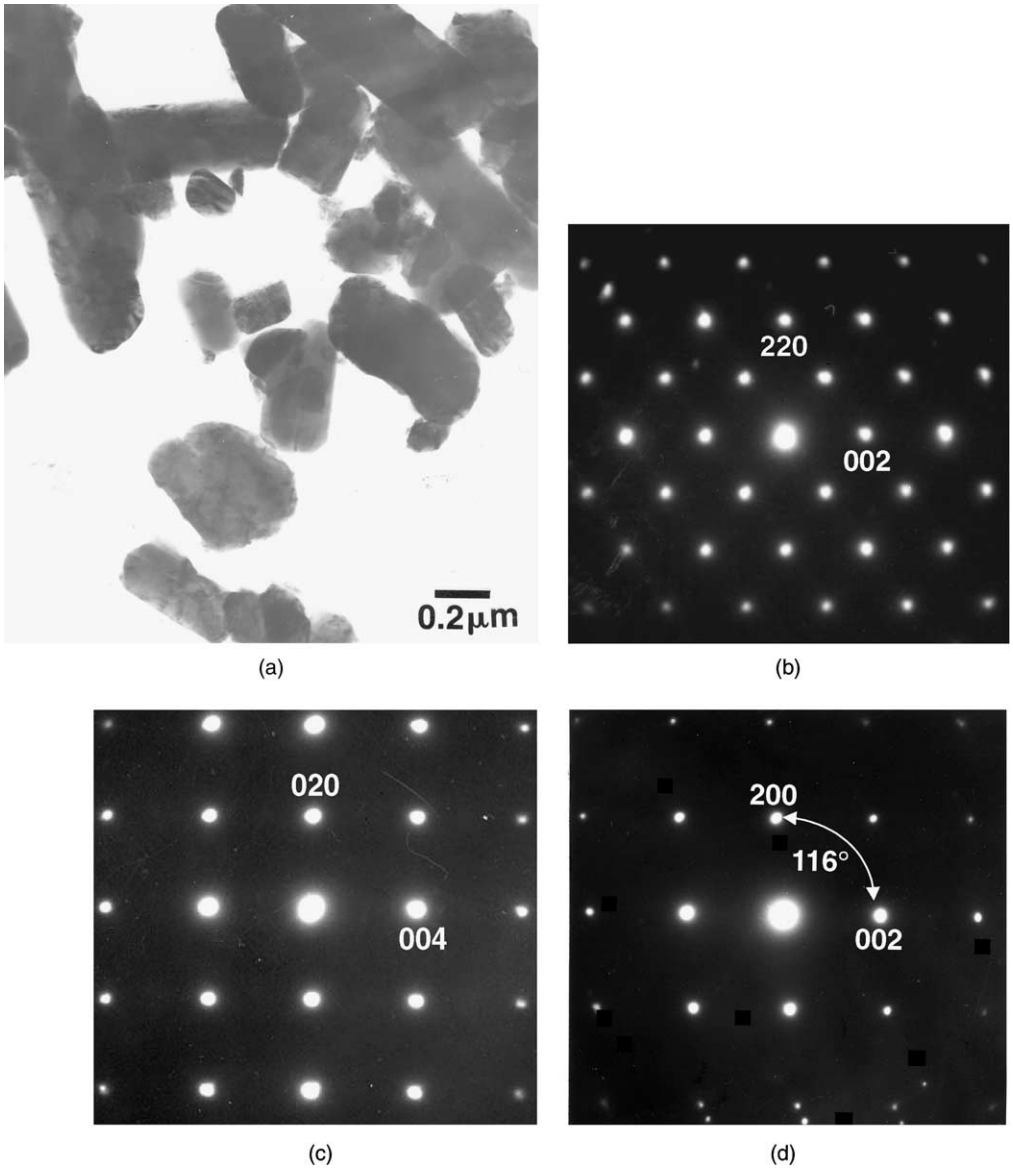

Fig. 5. (a) TEM bright field image of γ-$LiAl_{0.1}Mn_{1.9}O_4$ powder before cycling which show two types of particle shape in the powder; (b) electron diffraction pattern of a spinel phase in [1 1 0] zone; (c) tetragonal phase in [1 0 0] zone; (d) monoclinic particle in [0 1 0] zone.

assumed that t-$LiAl_{0.1}Mn_{1.9}O_4$ with smaller particle size is more susceptible to Jahn–Teller transformation during repeated Li-insertion cycles and to subsequent structural damage due to the high surface/volume ratio. The small particle size can also lead to particle growth or agglomeration during cycling, which can cause loss of electrical contact and capacity fade. Such detrimental particle growth has also been observed in the SnO_2 electrode for lithium secondary batteries [22]. In t-$LiAl_{0.1}Mn_{1.9}O_4$, the particle size has clearly increased from about 0.1 to 1 μm after 50 cycles, as suggested by the SEM image of t-$LiAl_{0.1}Mn_{1.9}O_4$ powder after cycling, shown in Fig. 8a, which could be another reason for the observed rapid loss of capacity.

Both j-$LiAl_{0.1}Mn_{1.9}O_4$ and γ-$LiAl_{0.1}Mn_{1.9}O_4$ powders have a lower proportion of the tetragonal or the monoclinic phase after cycling compared with the t-$LiAl_{0.1}Mn_{1.9}O_4$ powder, and show better capacity retention, as can be seen in Table 1. It is not clear how monoclinic phases are formed during cycling of j-$LiAl_{0.1}Mn_{1.9}O_4$. It is possible that the monoclinic phase we have found could be just a type of distorted $Li_2Mn_2O_4$ tetragonal structure. It is noted, however, that a $LiMnO_2$–spinel composite has been observed to improve the cycling behavior as compared with the pure spinel material [18,23]. There is no observable change in the particle size of the material after cycling, see Fig. 8c. The larger particle size could be responsible for the better capacity retention exhibited by the j-$LiAl_{0.1}Mn_{1.9}O_4$ material. In case of γ-$LiAl_{0.1}Mn_{1.9}O_4$ powder, Fig. 8c indicates that the elongated γ-$LiAl_{0.1}Mn_{1.9}O_4$ particles have broken up into equiaxed crystals during cycling. This suggests that

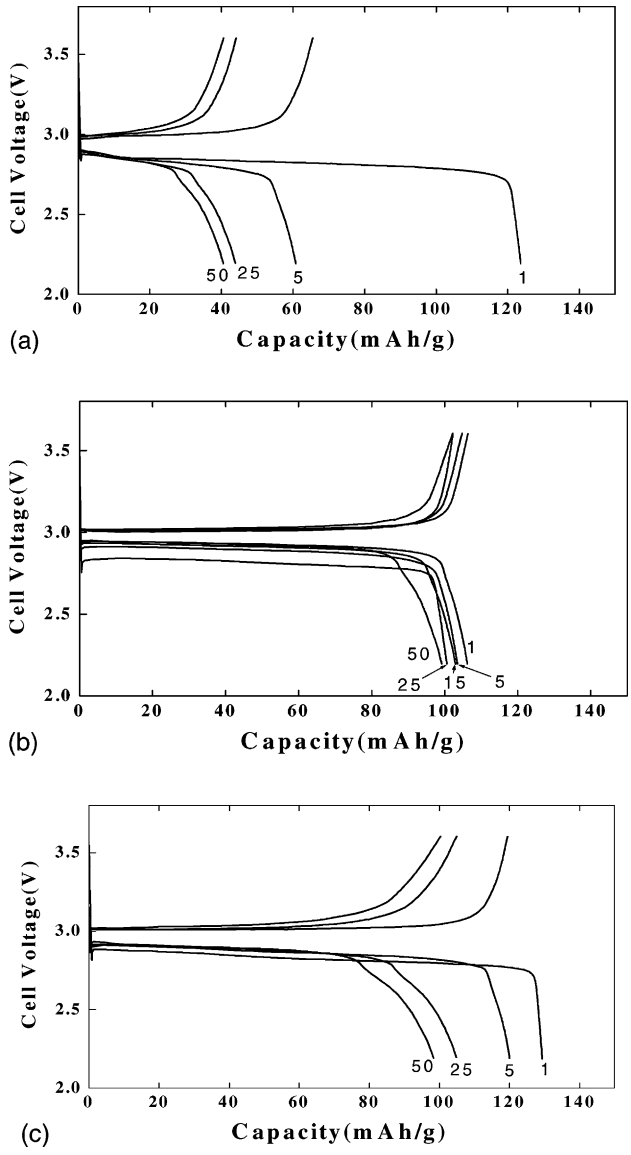

Fig. 6. Charge-discharge curves for $LiAl_{0.1}Mn_{1.9}O_4$|Li cell when cycled between 2.2 and 3.6 V: (a) t-$LiAl_{0.1}Mn_{1.9}O_4$; (b) j-$LiAl_{0.1}Mn_{1.9}O_4$; (c) γ-$LiAl_{0.1}Mn_{1.9}O_4$.

there is a substantial volume change during cycling. Such a change together with the volume expansion involved with the phase transition between initial $Li_2Mn_2O_4$ and $LiMn_2O_4$ could have led to the electrical disconnection of the cathode material, and the subsequent capacity loss for γ-$LiAl_{0.1}Mn_{1.9}O_4$.

Although all three powders show a phase change after cycling, the γ-$LiAl_{0.1}Mn_{1.9}O_4$ and t-$LiAl_{0.1}Mn_{1.9}O_4$ powders have undergone a significant change in volume fraction after cycling and show a relatively low discharge-capacity retention compared with the j-$LiAl_{0.1}Mn_{1.9}O_4$ powder. This fact suggests that the observed large volume change can further deteriorate the cycling performance of the spinel material at 3 V. It appears that there exists an optimum particle size at which the particle dissolution and volume change can be minimized when the spinel electrode is cycled at 3 V. In addition to the particle size, equiaxed shaped particles would be preferred to reduce the diffusion distance and to increase the stability of the particles during the Jahn–Teller distortion.

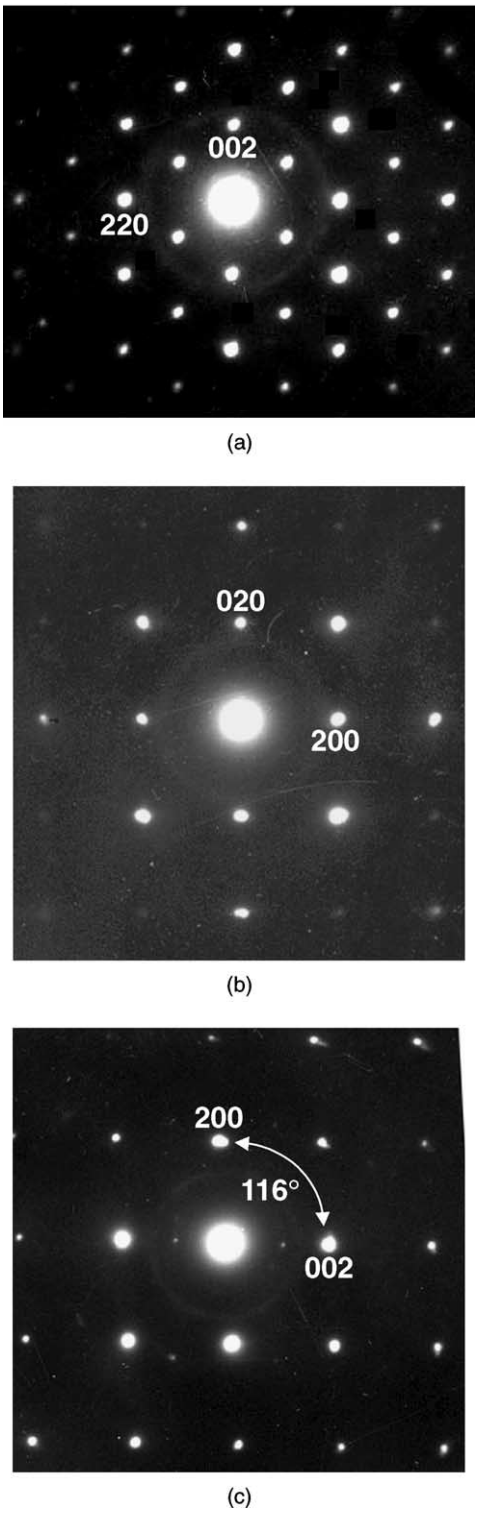

Fig. 7. Electron diffraction patterns for t-$LiAl_{0.1}Mn_{1.9}O_4$ particles after 50 cycles: (a) spinel phase in [1 1 0] zone; (b) tetragonal particle in [0 0 1] zone; (c) monoclinic particle in [0 1 0] zone.

4. Conclusions

Although XRD analysis indicate virtually no structural differences among the three powders produced from three different sources of manganese, TEM and SEM analysis reveal subtle differences in the microstructure, which result in different reversible capacity of electrochemical cell constructed using the three powders.

It has been found that control of the particle size and morphology is critical to ensure the minimal dissolution of the particles in the electrolyte and the detrimental large volume fraction change. Although we were unable to prove

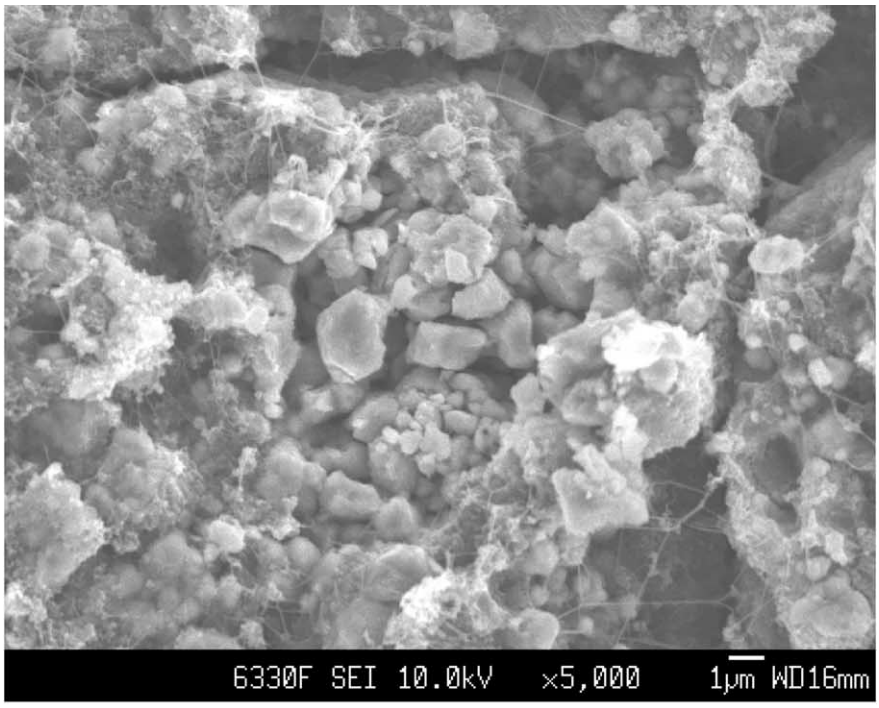

(a)

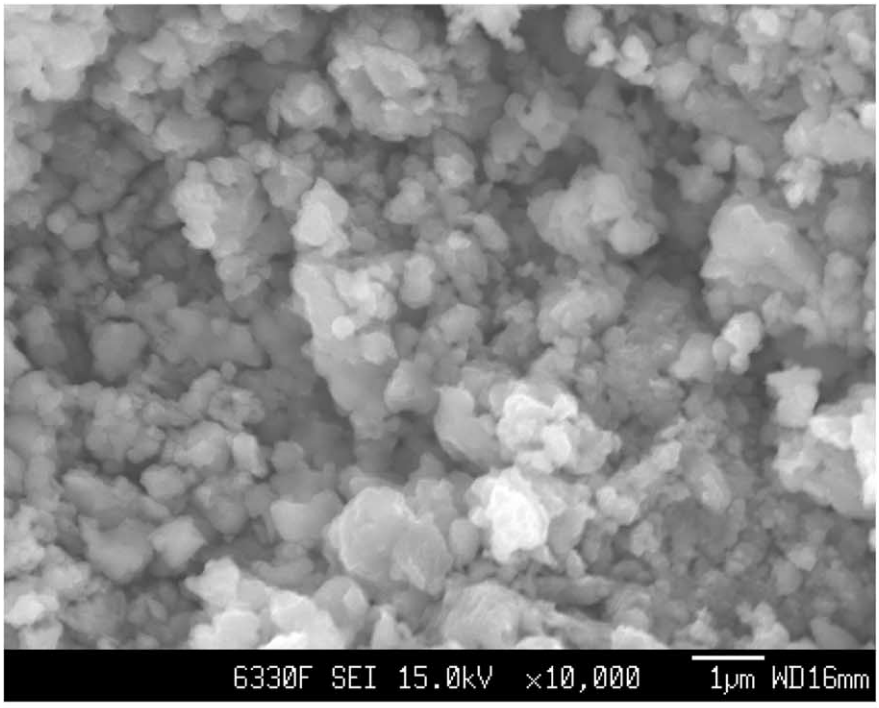

(b)

Fig. 8. SEM images of $LiAl_{0.1}Mn_{1.9}O_4$ powder after 50 cycles: (a) t-$LiAl_{0.1}Mn_{1.9}O_4$; (b) j-$LiAl_{0.1}Mn_{1.9}O_4$; (c) γ-$LiAl_{0.1}Mn_{1.9}O_4$.

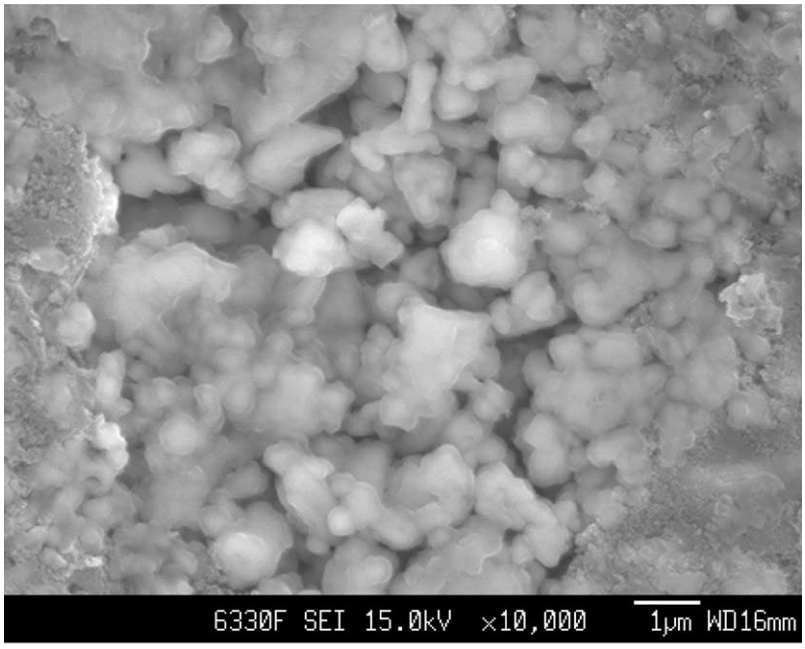

(c)

Fig. 8. (*Continued*).

how the monoclinic phase was formed during cycling of t-$LiAl_{0.1}Mn_{1.9}O_4$ and j-$LiAl_{0.1}Mn_{1.9}O_4$ powders, an investigation is underway to study the phase transformation of the material at different stages of the synthesis and electrochemical cycling.

Acknowledgements

The authors wish to acknowledge the partial financial support from the Hanyang University for this research.

References

[1] J.M. Tarascon, W.R. McKinnon, F. Coowar, T.N. Bowner, G. Amatucci, D. Guyomard, J. Electrochem. Soc. 141 (1994) 1421–1431.
[2] R.J. Gummow, A. de Kock, M.M. Thackerya, Solid State Ionics 69 (1994) 59–67.
[3] M.M. Thackery, A. de Koch, M.H. Rossow, D. Liles, J. Electrochem. Soc. 139 (1992) 363–366.
[4] D.H. Jang, J.Y. Shin, S.M. Oh, J. Electrochem. Soc. 143 (1996) 2204–2210.
[5] A. Yamada, J. Solid State Chem. 122 (1996) 160–165.
[6] J.M. Tarascon, E. Wang, F.K. Shokoohi, W.R. McKinnon, S. Colson, J. Electrochem. Soc. 138 (1991) 2859–2863.
[7] T. Ohzuku, M. Kitagawa, T. Hirayi, J. Electrochem. Soc. 137 (1990) 769–774.
[8] A.D. Roberston, S.H. Lu, W.F. Averill, W.F. Howard Jr., J. Electrochem. Soc. 144 (1997) 3500–3512.
[9] L. Guoha, H. Ikuta, T. Uchida, M. Wakihara, J. Elcetrochem. Soc. 143 (1996) 178–182.
[10] D. Zhang, B.N. Popov, R.E. White, J. Power Sources 76 (1998) 81–90.
[11] F. Le Cras, D. Bloch, M. Anne, P. Strobel, Solid State Ionics 89 (1996) 203–213.
[12] S.H. Park, K.S. Park, Y.K. Sun, K.S. Nahm, J. Electrochem. Soc. 147 (6) (2000) 2116–2121.
[13] D. Song, H. Ikuta, T. Uchida, M. Wakihara, Soild State Ionics 117 (1999) 151–156.
[14] Powerceli, CCP14 Homepage, http://www.ccp14.ac.uk.
[15] M.M. Thackeray, Prog. Solid State Chem. 25 (1997) 55.
[16] A. Yamada, K. Miura, K. Hinokuma, M. Tanaka, J. Electrochem. Soc. 142 (1995) 2149–2156.
[17] S.-H. Kang, J.B. Goodenough, J. Electrochem. Soc. 147 (2000) 3621–3627.
[18] Y. Shao-Horn, S.A. Hackney, A.R. Armstrong, R.G. Bruce, R. Gitzendanner, C.S. Johnson, M.M. Thackeray, J. Electrochem. Soc. 146 (1999) 2404–2412.
[19] T. Ohzuku, M. Kitagawa, T. Hirai, J. Electrochem. Soc. 137 (1990) 769–775.
[20] Y.-K. Sun, Y.-S. Jeon, Electrochem. Commun. 1 (1999) 597–599.
[21] M.M. Thackeray, J. Am. Ceram. Soc. 82 (1999) 3354–3374.
[22] R. Retoux, T. Brousse, D.M. Schleich, J. Electrochem. Soc. 146 (1999) 2472–2476.
[23] H. Wang, Y.I. Jang, Y.M. Chiang, in: Proceedings of the Symposium on Processing and Characterization of Electrochemical Materials and Devices, Vol. 109, American Ceramic Society, Cincinnati, OH, USA, 2000, p. 297.